Analysis of the Surface Energy Budget at a Site of GAME/Tibet using a Single-Source Model

Kun YANG, Toshio KOIKE

Department of Civil Engineering, The University of Tokyo, Tokyo, Japan

Hirohiko ISHIKAWA

Disaster Prevention Research Institute, Kyoto University, Kyoto, Japan

and

Yaoming MA

Cold and Arid Regions Environmental & Engineering Research Institute, Chinese Academy of Science, Beijing, China

(Manuscript received 9 January 2003, in final form 28 October 2003)

Abstract

In the GAME/Tibet project, the Anduo site is a typical plateau prairie area that is covered by short and sparse vegetation. From May to September 1998, we measured all the surface energy fluxes at this site to quantitatively describe the surface energy budget, but it was still questionable because of low energy closure ratios in most days of the rainy season.

To clarify the surface energy budget at this site, this study proposes a single-source energy partition model, to simplify the processes of heat and water vapor transfer from the surface. The model does not distinguish the contribution of turbulent fluxes from the vegetation, and the one from the ground, and thus has fewer parameters to be calibrated comparing to a dual-source model. The main model parameters are: the soil surface evaporation resistance, the parameter kB^{-1} (the logarithm of the ratio of the aerodynamic roughness length to the thermal roughness length), and the surface emissivity. Their values are calibrated by minimizing the discrepancy between measured and model-predicted values of soil temperatures.

This tuned single-source model is then validated by the agreement between the measured and simulated net radiation flux, surface soil heat flux, sensible heat flux, and latent heat flux on the days with high energy closure ratios. This model also reproduces these measured fluxes, except latent heat flux on the days with low closure ratios. The simulated latent heat flux is much higher than the measured one. We further show that the measured latent heat flux is untrustable due to an instrumental limitation, while the model provides a reasonable surrogate. Therefore, the single-source concept is applicable to the heat and water vapor transfer on the Tibetan plateau sparse-vegetation surface, and would contribute to a further research on the land-atmosphere interactions over the plateau.

Corresponding author: Kun YANG, River Lab, Dept. of Civil Engineering, University of Tokyo, Hongo 7-3-1, Bunkyo-ku, Tokyo 113-8656, Japan.
E-mail: yangk@hydra.t.u-tokyo.ac.jp

1. Introduction

The energy partition at a ground surface is one of the basic aspects of land-surface processes that affect climate and weather from the

regional scale to the global scale. The partition depends on many conditions such as the vegetation type, soil properties and atmospheric forces, but the incoming and outgoing energy at the ground surface maintain a balance. Therefore, the energy partition can be expressed simply as:

$$R_n = H + lE + G_0, \tag{1}$$

where H (Wm^{-2}) is the sensible heat flux into the atmospheric surface layer, lE (Wm^{-2}) is the latent heat flux, and G_0 (Wm^{-2}) is the surface soil heat flux. R_n (Wm^{-2}) denotes the net radiation flux, which is the difference between the downward and upward radiation fluxes.

In recent years, however, many researchers have reported on the energy closure problem at the ground surface, given that turbulent heat fluxes are measured by the eddy-correlation method. That is, the observed net radiation is usually greater than the sum of the observed sensible heat, the latent heat and the surface soil heat. Nie et al. (1992) found that the maximum residual energy could reach 160 Wm^{-2} during the First ISLSCP (International Satellite Land Surface Climatology Project) Field Experiment (FIFE), and that eddy correlation systems gave slightly lower latent heat fluxes in comparison with the Bowen ratio systems. McCaughey et al. (1997) reported that the average daily energy budget closure $(H + lE)/(R_n - G_0)$ varied from 0.85 to 0.95 for forest sites of the BOREAS (Boreal Ecosystem-Atmosphere Study) experiment. Twine et al. (2000) suspected that the sum of the sensible and latent heats might be under-measured by the eddy-correlation method, and therefore some corrections need to be made to these terms. Lamaud et al. (2001) showed that the energy budget closure was quite satisfactory above the understorey of a pine forest once all of the storage terms in the soil, canopy and canopy air space were included in the budget equation.

The lack of energy closure is particularly noticeable in the Tibetan Plateau during the Asian summer monsoon, based on the observations of the GAME/Tibet (GEWEX Asia Monsoon Experiment in the Tibetan Plateau) and the TIPEX (Tibetan Plateau Experiment of Atmospheric Sciences) projects of 1998. As an example, Fig. 1 shows the daily average incoming and outgoing energy fluxes at the Naqu Flux (FX) site and the MS3478 site of the GAME/Tibet, where the residual energy $R_n - (G_0 + H + lE)$ often exceeded one third of the net radiation. Similar large residual values were also found at other sites in the plateau (Ishikawa et al. 1999; Bian et al. 2002). Ishikawa et al. (1999) pointed out that the closure problem mainly occurred in the afternoon and that the residual energy was greater than those reported in the FIFE and the BOREAS. Miyazaki et al. (2000) suggested that the amount of residual energy in the plateau was larger in the monsoon period than in the pre-monsoon period. The energy closure problem can not be explained by topographic heterogeneity, canopy energy storage or insufficient fetch, because the surfaces at these plateau sites are sufficiently wide and flat, and the vegetation is short. Ta-

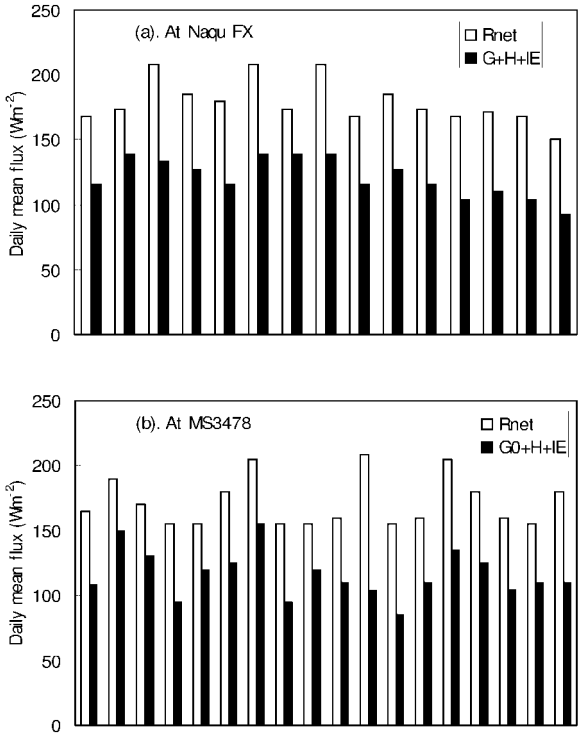

Fig. 1. Comparison between daily average incoming and outgoing energy fluxes. (a) at Naqu FX for 15 clear days from July–September, 1998 (Wang et al. 1999), (b) at MS3478 for August, 1998 (Miyazaki et al. 2000).

naka et al. (2001a) pointed out that the soil heat flux might be under-measured if the melting process of the frozen soil water is not taken into account. Wang et al. (1999) suggested that the measurement error in the latent heat flux may contribute significantly to the energy closure problem at the Naqu Flux site; however, Kim et al. (2001) contested that the net radiation flux and the latent heat flux were the least erroneous, while the soil heat flux and the sensible heat flux were the most error-prone for the same site. These opposite conclusions result from the use of different evaluation methods but also from some uncertainties caused by incomplete observations.

Since the overall goal of GAME/Tibet is to investigate the land-atmosphere interactions in the context of the Asian summer monsoon system, it is of primary importance to clarify the surface energy budget and to provide reliable data for land-atmosphere interactions and hydrological studies, such as flux parameterizations and subsurface processes modeling. For this purpose, this study will propose a single-source energy partition model to investigate the surface energy budget on a plateau site, evaluate the reliability of measured energy fluxes, and provide a surrogate of energy fluxes if the measurements are not trustable. The site of interest is the Anduo site of the GAME/Tibet project. It is a typical plateau site, where it is covered by sparse and short grasses.

This study first describes the measured surface energy budget at the Anduo site. Systematic measurements were carried out during the IOP (intensive observing period) of 1998 (from May to September). In order to investigate the surface energy budget, we present a single-source energy partition model and calibrate model parameters by minimizing the discrepancy between the measured and model-predicted soil temperatures. Various sensitivity studies of the energy partition are then carried out. Finally, using the simple biosphere model SiB2 (Sellers et al. 1996a), we analyze the vegetation effect on the energy partition through which the single-source energy partition model is justified.

Note that local solar time is used throughout the work, which is approximately 6 hours earlier than the Coordinated Universal Time (UTC).

2. Description of the site and experimental data

The Anduo site is located in the central Tibetan Plateau (Lat. 32.241°N, Lon. 91.635°E), where the elevation is 4700 m ASL. Its surface is essentially flat and open. During the pre-onset of the Asian summer monsoon (around the beginning of June), the surface is very dry and covered by dry grasses; after the onset, the surface becomes wet, and the grasses grow after June. Because of the harsh plateau climatic conditions, the grasses grow slowly and their growing period is less than 2 months. The grasses are sparse and very short (several centimeters), and the leaves are slender (several millimeters). Table 1 shows the temporal variation in the aerodynamic roughness length z_0, *NDVI* (Normalized Difference Vegetation Index), and *LAI* (Leaf Area Index) at this site. The roughness length z_0 is derived based on the AWS data (see Figure 3 in Yang et al. 2003), and corresponds well to the variation of *NDVI* and *LAI*. The *NDVI* is interpolated from monthly mean values, and the *LAI* is derived from *NDVI* according to Asrar et al. (1984), as shown below:

$$LAI = -\ln((1 - NDVI/0.915)/0.83)/0.96. \quad (2)$$

Table 2 shows laboratory experiment results based on five soil samples from the Anduo site. ρ_{dry} is the bulk density of dry soil, θ_{sat} is the volumetric saturation water content, θ_{rsd} is the

Table 1. Vegetation parameters at Anduo.

DOY	*NDVI*	*LAI*	z_0 (m)
130	0.16	0.00	N/A
140	0.16	0.00	N/A
150	0.16	0.00	0.0013
160	0.17	0.02	0.0013
170	0.21	0.08	0.0014
180	0.29	0.20	0.0016
190	0.33	0.27	0.0016
200	0.37	0.35	0.0016
210	0.39	0.38	0.0020
220	0.40	0.40	0.0020
230	0.40	0.40	0.0025
240	0.38	0.36	0.0021
250	0.36	0.33	0.0022
260	0.32	0.25	N/A

Table 2. Soil parameters at Anduo.

Depth (cm)	ρ_{dry} (g cm^{-3})	θ_{sat} m^3 m^{-3}	θ_{rsd} m^3 m^{-3}	K_{sat} (cm s^{-1})	ψ_{sat} (cm)	b
5	0.667	0.633	0.143	N/A	−3.464	5.296
5	0.817	0.593	0.170	0.003561	−11.402	5.685
20	1.378	0.440	0.106	0.004883	−6.665	4.855
20	1.694	0.318	0.126	0.000210	−10.678	8.207
60	1.426	0.370	0.073	0.002773	−5.973	4.313

residual water content corresponding to 200 m suction, K_{sat} is the saturation hydraulic conductivity, ψ_{sat} is the "saturation" water potential, and b is the slope of the water retention curve. The top layer has much lower ρ_{dry} and much higher θ_{sat} and θ_{rsd} than the layer below. This apparent vertically heterogeneous structure is caused by vegetation roots, which extend to a depth of near 20 cm and share 40 percent of the volume of the top layer.

The field measurements at Anduo in the GAME/Tibet IOP comprise: (1) soil moisture θ_s at six depths (4, 20, 60, 100, 160 and 258 cm) measured using a TDR system (Trime MUX); (2) soil temperature T_s at twelve depths (4, 5, 10, 20, 40, 60, 80, 100, 130, 160, 200 and 279 cm) measured using thermometers (Pt-100); (3) soil heat flux G at depths of 10 and 20 cm using a heat-plate (EKO MF-81); (4) downward shortwave radiation $R^{\downarrow}_{sw}$ and upward shortwave radiation $R^{\uparrow}_{sw}$ using EKO MS-801, downward longwave radiation $R^{\downarrow}_{lw}$ and upward longwave radiation $R^{\uparrow}_{lw}$ using Eppley PIR; (5) sensible heat flux H_{obs}, latent heat flux lE_{obs}, and momentum flux τ_{obs} at a height of 2.85 m above the ground measured by a fast response system consisting of a 3-D sonic anemo-thermometer (Kaijo DA-300) and an infrared open-path hygrometer (Kaijo AH-300). In the post-processing of the turbulence data, various corrections were made, which include cross wind and humidity effects on temperature, dynamic calibration and corrections due to low frequency instability for humidity, and the Webb et al. (1980) correction for fluxes (Tamagawa 1999); (6) The AWS (Automated Weather Station) measurements: wind U_a measured using an vane, temperature T_a using a Pt-100, and water vapor q_a measured using the electric capacitance; and (7) precipitation measured using tipping buckets.

In this study, we selected measurements for the whole August 1998 to analyze the surface energy budget and its closure ratio, because of (1) the available successive data series including soil moistures and temperatures, the 4-component radiation, the eddy-correlation measured turbulent fluxes, and the mean meteorological quantities; (2) the large observed unclosed energy, (3) no freezing and thawing processes. Item (3) is important because including the frozen soil processes would complicate the energy budget.

Figures 2a and 2b, respectively, show the measured soil water content and soil temperature profiles during this period. It is noticeable that the plateau surface is very wet during August. Note that the measured soil water content at 4 cm is corrected considering the high organic matter content and low bulk density. The soil moisture was measured by TDR based on the following Topp et al. (1980) empirical function between the apparent dielectric constant K_a, and the volumetric water content θ:

$$K_a = 3.03 + 9.3\theta + 146.0\theta^2 - 76.7\theta^3. \quad (3)$$

This relationship is usually independent of soil type. However, Roth et al. (1992) and Jacobsen and Schjønning (1993) indicate that a different calibration is required for soils with high organic matter contents and low bulk densities, which is the case in the top soil layer at our site. Therefore, the measurement at 4 cm is corrected following the relationship of Roth et al. (1992):

$$K_a = 0.97 + 10.9\theta + 87.4\theta^2 - 28\theta^3. \quad (4)$$

The corrected value of the soil water content at 4 cm is 0.10 higher than the measured value, so the correction cannot be neglected.

3. Soil heat flux and observed energy partition

3.1 Estimate soil heat flux

To evaluate the observed energy partition, the surface soil heat flux must first be reliably estimated. The soil heat flux at a depth is calculated based on the measured soil moisture and soil temperature profiles as follows:

$$G_{z_1} = -\lambda_s \frac{\partial T_s}{\partial z}\bigg|_{z_2} + \int_{z_1}^{z_2} \rho_s c_s \frac{\partial T_s}{\partial t} dz, \quad (5)$$

$$\rho_s c_s = \rho_{dry} c_{dry} + \rho_w c_w \theta, \quad (6)$$

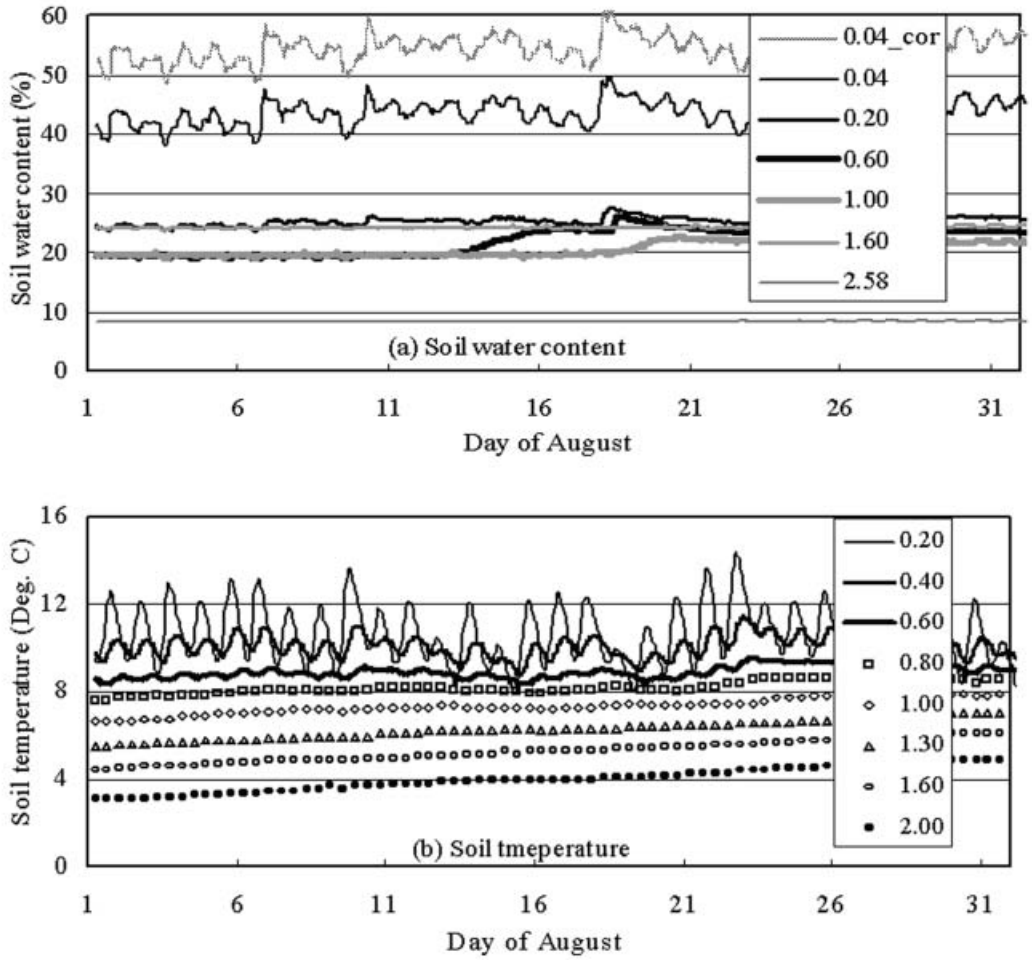

Fig. 2. Soil moisture and soil temperature measured at the Anduo site during August, 1998. The symbol 0.04_cor in (a) refers to the corrected soil moisture at 4 cm.

where z_1 (m) and z_2 (m) are soil depths (positive if downward), and G_{z_1} is the soil heat flux at z_1 (positive if downward). $\rho_{dry}c_{dry}$(Jkg^{-1} m^{-3}) is the bulk heat capacity of dry soil, and $\rho_w c_w = 4.195 \times 10^6$ Jm^{-3} K^{-1}.

The first term on the right hand side of Eq. (5) is the soil heat flux at z_2. If z_2 is much deeper than z_1, then the soil heat flux at z_2 becomes much smaller than that at z_1, and thus the uncertainty in the first term is negligible. Therefore, we set $z_2 = 1.6$ m and calculate the temperature gradient at z_2 from the observations at the depths of 1.6 m and 2.0 m, where the temperature varies slowly.

The second term is then integrated from z_2 to z_1. The bulk heat capacity of the dry soil in this term can be estimated from the saturation water content as in SiB2:

$$\rho_{dry}c_{dry} = 0.5(1 - \theta_{sat})\rho_w c_w, \tag{7a}$$

or from the bulk density of dry soil ρ_{dry} as given by the Global Soil Data Task (IGBP-DIS CD-ROM, 1999):

$$\rho_{dry}c_{dry} = (0.076 + 0.748\rho_{dry}/\rho_w) \times 10^6 \text{ Jm}^{-3} \text{ K}^{-1}. \tag{7b}$$

The soil temperature profile in Eq. (5) is interpolated to computational grids following two steps. Step 1 is to solve the thermal diffusion equation. Given the skin radiative temperature and deep temperature as the boundary conditions, the equation is solved with an assumed constant thermal conductivity to obtain the

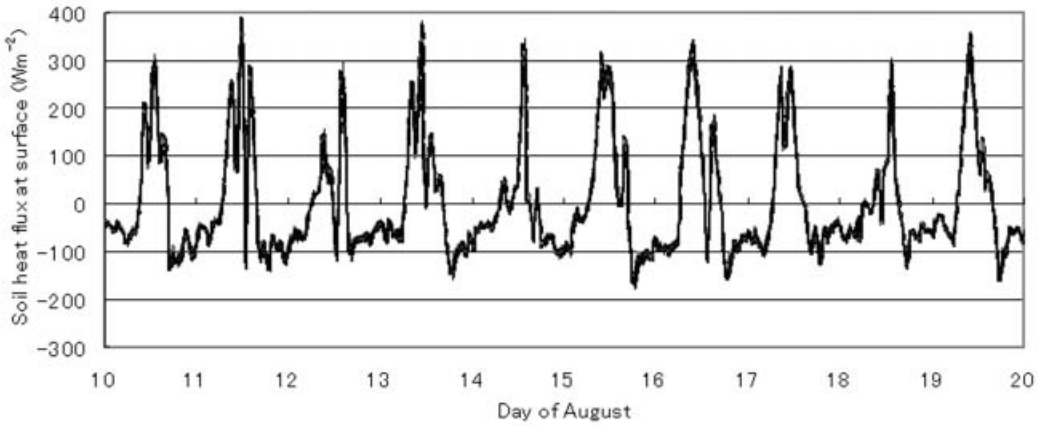

Fig. 3. Comparison of the derived soil heat flux among uncertainty tests (see the text) for August, 1998.

temperature at the grids. The skin radiative temperature is derived from the upward longwave $R_{lw}^{\uparrow}$, given the surface emissivity $\varepsilon_g = 0.988$ (The value will be justified in Section 4). Strictly speaking, the skin temperature T_{sfc} differs from the ground temperature T_g due to the vegetation effect, but the difference may be negligible because the vegetation coverage and leaf area index are so low at this site. As will be shown in Section 6, the difference $T_g - T_{sfc}$ seldom exceeds 1 K, even at noon, so it is reasonable to use the skin radiative temperature as the upper boundary condition. Step 2 is to correct the simulated temperature profile. If the simulated profile is different from the observed one, the simulated one is then corrected by interpolating their difference to each grid. Because the difference is usually small, a linear or spline interpolation is acceptable.

The soil moisture profile in Eq. (6) is interpolated linearly. As shown in Fig. 2a, the soil moisture in the layer from 0.2 m to 1.6 m varies from 0.20–0.25; and thus linear interpolation does not cause any severe problems. However, the soil moisture above 0.2 m experiences a rapid transition that is related to the vertical soil heterogeneity shown in Table 2. Because the heat into the soil surface is mainly stored in the top layer, its estimation might be sensitive to the interpolation of θ and θ_{sat} in the top layer. Therefore, two cases are tested. In one case, we assume that θ and θ_{sat} are uniform above 0.04 m, and then vary linearly between 0.04 m and 20 cm. In the other case, θ and θ_{sat} are uniform above 0.10 m, and then then vary linearly between 0.10 m and 20 cm.

Figure 3 shows the derived surface soil heat flux of several uncertainty tests, which combine different formulas for heat capacity [Eq. (7a) or (7b)], thermal conductivity ($\lambda_s = 0.5$ or 1.0 $\mathrm{Wm^{-1}\ K^{-1}}$), and interpolation of the soil moisture. The heat flux is almost insensitive to thermal conductivity and soil moisture interpolation, and the relative difference caused by Eq. (7a) and (7b) is about 8% in the daytime, therefore the derived surface soil heat flux is not so sensitive to these uncertainties.

On the other hand, if we consider the accuracy of soil moisture measurements (~ 0.03 $\mathrm{m^{-3}\ m^{-3}}$), the estimation of the soil heat flux may result in an error of about 6%. The accuracy of subsurface temperature measurements is as high as 0.1 K, thus it does not yield significant uncertainties. The surface temperature difference $T_g - T_{sfc}$ is generally less than 1 K, which only causes underestimations of several $\mathrm{Wm^{-2}}$ in the surface soil heat flux. Therefore, the estimated surface soil heat flux can be used as a surrogate of the measurement with an uncertainty of no more than 10%.

Figures 4a and 4b show a comparison between the derived and measured soil heat fluxes measured using heat-plates at 10 cm and 20 cm. They show that the derived flux follows the phase of the measured flux, while the amplitude of the derived flux is much larger than that of the measured flux. This does not mean a big error in the estimation of the soil heat flux.

Instead, the fluxes measured by the heat-plate should be corrected because of the difference in the thermal conductivity between the heat-plate and the soil. According to Philip (1961),

$$\frac{G_m}{G_s} = \frac{1}{1 - \alpha(1 - \lambda_s/\lambda_{meff})d_{eff}/A^{1/2}}, \quad (8)$$

where G_m/G_s is the ratio of the mean flux through the heat-plate to the flux through the soil, λ_{meff}/λ_s is the ratio of the heat-plate effective conductivity to the soil conductivity, α is a constant, d_{eff} is the heat-plate effective thickness in the general direction of heat flow, and A is the area of the mean cross section of the heat-plate.

At the Anduo site, the heat-plate conductivity is $\lambda_m = 0.21$ Wm^{-1} K^{-1}, the thickness is $d =$ 4 mm, and the area is $A = 20$ mm $\times$ 110 mm. λ_s is derived by minimizing the heat flux difference $(-\lambda_s \partial T_s/\partial z - G_s)^2$ using the least-square method, which gives 1.42 Wm^{-1} K^{-1} for a depth of 10 cm and 2.05 Wm^{-1} K^{-1} for a depth of 20 cm. Philip (1961) gives $\alpha = 1.7$ for a thin circular plate and a square plate, and this value is used in the correction. λ_{meff} and d_{eff} are affected by the heat-plate and the air gap between the soil and the heat-plate surfaces. Increasing the air gap would decrease λ_{meff} and increase d_{eff} of the heat-plate. As in Philip (1961), the air gap is assumed to be 1/20 of the thickness of the plate, both above and below the plate. Given this, $d_{eff} = 1.1d$ and $\lambda_{eff} = 11\lambda_{air}\lambda_m/(10\lambda_{air} + \lambda_m)$. With the air thermal conductivity $\lambda_{air} = 0.025$ Wm^{-1} K^{-1}, one gets $\lambda_{meff} = 0.125$ Wm^{-1} K^{-1}. The soil heat flux is then corrected with these parameters.

Figures 4a and 4b shows that the corrected soil heat fluxes at 10 cm and 20 cm are compa-

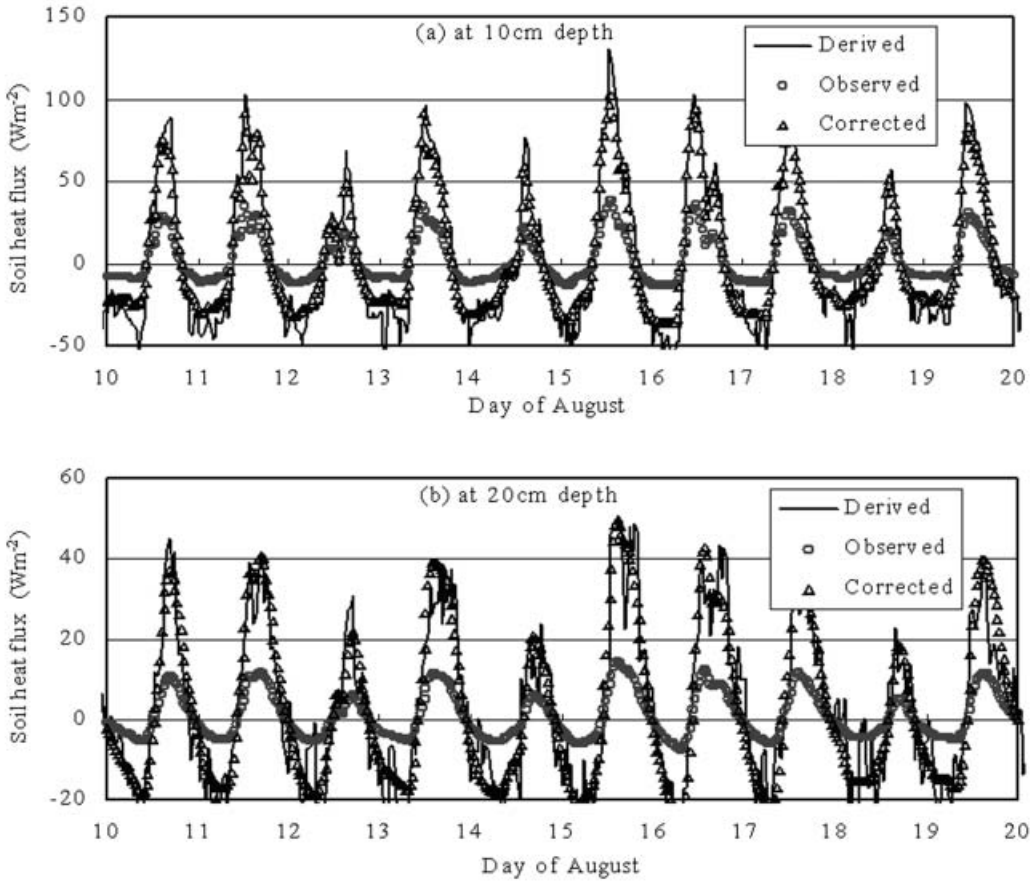

Fig. 4. Comparison between the observed, corrected and derived soil heat flux.

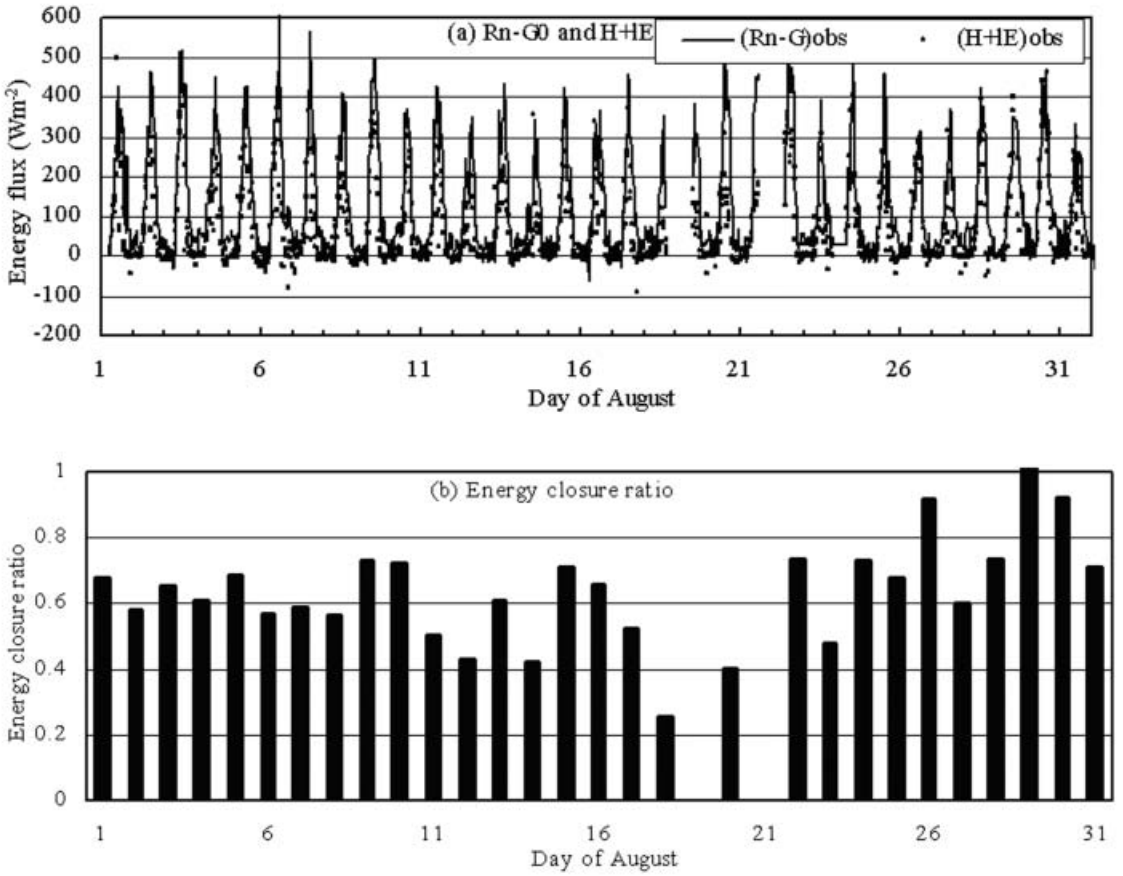

Fig. 5. The observed energy partition (a) and closure ratio during 10LT–16LT (b) in August, 1998.

rable to the one derived from Eq. (5). Even so, caution needs to be taken with regard to this correction because it is sensitive to the air gap.

3.2 Energy closure ratio

Using the measured sensible heat, the latent heat, the shortwave radiation, the longwave radiation, and the above-derived surface soil heat flux, the residual energy on the surface is calculated as follows

$$E_{robs} = (R_n - G_0)_{obs} - (H + lE)_{obs}, \qquad (9)$$

where $R_n = (R_{sw}^{\downarrow} + R_{lw}^{\downarrow}) - (R_{sw}^{\uparrow} + R_{lw}^{\uparrow})$, calculated from the measurements of four radiation fluxes.

Figure 5a shows the energy flux $R_n - G_0$ and $H + lE$, and Fig. 5b shows the mean energy closure ratio $(H + lE)/(R_n - G_0)$ during 10LT–16LT for each day in August. The mean values of $H + lE$ and $R_n - G_0$ during 10LT–16LT are 188.6 Wm^{-2} and 301.7 Wm^{-2}, respectively. The hourly mean residual flux is frequently more than 200 Wm^{-2} and occasionally more than 300 Wm^{-2} at noon and in the early afternoon. The mean closure ratio during 10LT–16LT is as low as 0.64. However, the ratio before August 23 is obviously less than afterwards. The difference will be discussed in Section 7. The measurement of the net radiation is believed to be the least error-prone, and the surface soil heat flux is derived reasonably from the above. So the low energy closure ratio must result from errors in the sensible heat and/or the latent heat.

4. Surface energy budget from a single-source model

Because the plateau vegetation is sparse and very short, the surface energy partition can be approximated by a single-source model described below. The approximation will be justi-

fied in Section 6. The single-source (the heat is from a single surface) model has significantly fewer parameters than a dual-source (the heat is from vegetation and the ground) model, and thus its model parameters can be calibrated more easily. In this section, we will present the model and calibrate the model parameters, and then use it to analyze the surface energy partition. Because we are to address the surface energy partition rather than the water budget, the measured soil water content will be supplied as input data.

4.1 Energy partition model

The turbulent heat fluxes in a surface layer can be estimated as follows:

$$H = \rho c_p(\Theta_{sfc} - \Theta_a)/R_a, \tag{10}$$

$$lE = \rho l(q_{sfc} - q_a)/(R_a + R_s), \tag{11}$$

where ρ (kgm^{-3}) is the air density, c_p (Jkg^{-1} K^{-1}) is the air specific heat, and l (Jkg^{-1}) is the vaporization heat. Θ_{sfc} (K) and Θ_a (K) are, respectively, the surface radiative potential temperature and the air potential temperature at a reference level. q_{sfc} (kg kg^{-1}) is the equilibrium specific humidity at the surface, and q_a (kg kg^{-1}) is the air humidity at the reference level. R_a is the aerodynamic resistance for heat transfer, and R_s is the soil surface resistance for evaporation.

The resistance R_a is calculated using the profile-flux relationship described by Monin-Obukohv's similarity theory, which is given by:

$$R_a = \frac{Pr_0}{k^2 U}\left(\ln\frac{z_m}{z_0} - \psi_m\left(\frac{z_0}{L}, \frac{z_m}{L}\right)\right) \times \left(\ln\frac{z_h}{z_T} - \psi_h\left(\frac{z_T}{L}, \frac{z_h}{L}\right)\right), \tag{12}$$

$$\psi_m(z_0/L, z_m/L) = \int_{z_0/L}^{z_m/L} \frac{1-\phi_m(z/L)}{z/L} d(z/L), \tag{13}$$

$$\psi_h(z_T/L, z_h/L) = \int_{z_T/L}^{z_h/L} \frac{1-\phi_h(z/L)/Pr_0}{z/L} d(z/L), \tag{14}$$

where z_0 (m) is the aerodynamic roughness length, z_T (m) is the thermal roughness length, z_m (m) is the reference level of the wind speed measurement, z_h (m) is the reference level of the temperature and humidity measurement, Pr_0 is the Prandtl number, L (m) is the buoyancy length, and ϕ_m and ϕ_h are stability functions corresponding to wind speed and temperature.

The aerodynamic roughness length z_0 is shown in Table 1, and the thermal roughness length in the temperature equation is generally estimated as

$$z_T = z_0 \exp(-kB^{-1}). \tag{15}$$

In general, the parameter kB^{-1} varies with surface and atmospheric conditions, and is determined empirically. The stability functions ϕ_m and ϕ_h have the general form:

$$\phi_m(z/L) = \begin{cases} 1+\beta_m z/L & z/L \geq 0 \\ (1-\gamma_m z/L)^{-1/4} & z/L < 0 \end{cases}, \tag{16a}$$

$$\phi_h(z/L) = \begin{cases} Pr_0(1+\beta_h z/L) & z/L \geq 0 \\ Pr_0(1-\gamma_h z/L)^{-1/2} & z/L < 0 \end{cases}, \tag{16b}$$

where $\beta_m, \beta_h, \gamma_m, \gamma_h$ and Pr_0 are coefficients.

Högström (1996) suggested $\beta_m = 5.3$, $\beta_h = 8.0$, $\gamma_m = 19.0$, $\gamma_h = 11.6$ and $Pr_0 = 0.95$. These values are adopted in this study. To improve the computational efficiency, which is important for the below-mentioned optimization procedure, Yang et al. (2001) proposed an analytical solution of the unknown z/L if the stability functions Eqs. (16a–16b) are used. For a stable surface layer, its exact solution is

$$z/L = (-b - \sqrt{b^2 - 4ac})/2a. \tag{17}$$

For an unstable layer, an approximate solution is used:

$$z/L = \left(\frac{Ri_b}{Pr_0}\frac{(\ln(z/z_0))^2}{\ln(z/z_T)}\left(\frac{z}{z-z_0}\right)\right) \Big/ \left(1 - \frac{Ri_b}{Pr_0}\frac{\gamma_m^2}{8\gamma_h}\frac{(1-z_0/z)}{(1-z_T/z)}p\right), \tag{18}$$

where Ri_b is the bulk Richardson number, and a, b, c and p are functions of $z/z_0, z/z_T$ and Ri_b, and can be found in Yang et al. (2001).

The soil surface resistance R_s is a function of the soil type and is formulated as an exponential form in some studies (Kondo 1994; Sellers et al. 1996a). Thus we assume

$$R_s = \exp(c_1 - c_2\theta_e), \tag{19}$$

where c_1 and c_2 are two constants depending on the soil type. $\theta_e = (\theta - \theta_{rsd})/(\theta_{sat} - \theta_{rsd})$ is the soil wetness.

The surface specific humidity is calculated using

$$q_{sfc} = rh_{sfc} q_{sat}(T_g), \tag{20}$$

where $rh_{sfc} = \exp(\psi_{sfc} g / R_w T_g)$ is the equilibrium relative humidity in the surface layer. Here, ψ_{sfc} (m) is the surface water potential, $g = 9.81\ \mathrm{ms}^{-2}$, and $R_w = 461.5\ \mathrm{Jkg}^{-1}\ \mathrm{K}^{-1}$.

The soil temperature profile is calculated by the thermal diffusion equation as follows:

$$\frac{\partial \rho_s c_s T_s}{\partial t} = \frac{\partial}{\partial z}\left(\lambda_s \frac{\partial T}{\partial z}\right). \tag{21}$$

The upper boundary condition is the surface heat flux condition:

$$G_0 = R_{net} - H - lE, \tag{22}$$

$$R_n = R^{\downarrow}_{sw} + R^{\downarrow}_{lw} - R^{\uparrow}_{sw} - \varepsilon_g \sigma T^4_{sfc}, \tag{23}$$

where ε_g is the surface emissivity, and $\sigma = 5.67 \times 10^{-8}\ \mathrm{Wm}^{-2}\ \mathrm{K}^{-4}$ is Stefan-Boltzmann constant.

The lower boundary condition is $T(z_l) = T^m(z_l)$, where $T^m(z_l)$ is the measured temperature at the lower boundary z_l.

The algorithm to run the model is as follows: (1) given the parameters $kB^{-1}, \lambda_s, R_s, \varepsilon_g$, and the soil temperature and moisture profiles at the initial time; (2) calculate the resistance R_a using Eq. (12), R_s using Eq. (19), and q_{sfc} using Eq. (20); (3) calculate the heat flux and evaporative flux according to Eqs. (10)–(11); (4) calculate the surface soil heat flux G_0; (5) calculate the soil temperature profile using the finite difference method; (6) update the soil moisture profile according to the observations; (7) go to step (2) until the end of the model time.

4.2 Cost function

In the above model, there are four parameters to be determined: the parameter kB^{-1}, the soil surface resistance R_s (or c_1 and c_2), the soil thermal conductivity λ_s, and the surface emissivity ε_g. The soil thermal conductivity λ_s can be derived from the soil heat flux and the soil temperature profile, which gives $\lambda_s = 1.14\ \mathrm{Wm}^{-1}\ \mathrm{K}^{-1}$ at the surface and $1.42\ \mathrm{Wm}^{-1}\ \mathrm{K}^{-1}$ at 10 cm. A linear variation of λ_s from the surface to a depth of 10 cm is assumed. The surface emissivity ε_g and parameter kB^{-1} are assumed to be constant because the change in the surface features is insignificant throughout August. Their values are optimized as described below.

Given the initial value of each parameter, we first solve the temperature profile in the top 10 cm with the observed soil temperature at a depth of 10 cm as the lower boundary condition. To model the soil temperature accurately, 20 uneven grids are used in the model domain, with thinner grids near the surface and coarser grids in the deeper layer. We then minimize the below-defined difference between the observed and model-predicted values of soil temperature T_{sfc} and $T_{5\,\mathrm{cm}}$:

$$F = \sqrt{\frac{1}{t_m}\sum_{t_i=1}^{t_m}\left(\frac{\left(T^m_{sfc}(t_i) - T^p_{sfc}(t_i)\right)^2}{AT^2_{sfc}} + \frac{\left(T^m_{5\,\mathrm{cm}}(t_i) - T^p_{5\,\mathrm{cm}}(t_i)\right)^2}{AT^2_{5\,\mathrm{cm}}}\right)}, \tag{24}$$

where t_m is the number of measurements over time, and AT is the amplitude of the diurnal variation of the soil temperature. Superscripts 'm' and 'p' represent measurements and predictions, respectively.

It is noted that the above optimization automatically makes the simulated upward longwave radiation and soil heat flux consistent with the measurements.

4.3 Optimization technique: simulated annealing

Because there are multiple model parameters to be optimized, and the cost function is highly non-linear and contains many local minima, we use a so-called simulated annealing algorithm to find the global minimum of the cost function, which has been proved effective for optimization problems with a number of variables in many applications (e.g., Szu and Hartley 1987; Dougherty and Marryott 1991). Simulated annealing is based on the analogy between solid annealing and the searching process of an optimization problem, so it is a heuristic optimization method. The readers can find details in Kirkpatrick et al. (1983).

4.4 Surface energy partition

Using data for the first 10 days of August, the values of the parameters are optimized. The optimal values are shown in Table 3, corresponding to Case 1. The other cases in the table correspond to several sensitivity studies discussed in Section 5. The optimal value of

Table 3. Optimized soil and aerodynamic parameters.

	Case 1	Case 2a	Case 2b	Case 3a	Case 3b
Parameter					
kB^{-1}	3.545	3.508	3.530	3.882	2.975
c_1	6.582	5.753	7.827	7.323	5.515
c_2	4.387	3.126	5.677	5.164	2.499
ε_g	0.989	0.989	0.989	0.989	0.990
Cost function					
F	0.0438	0.0440	0.0445	0.0470	0.0435

the surface emissivity is close to that which we used for converting the surface temperature from the upward longwave radiation in Section 3.

With these optimized parameters, we use the single-source model to simulate the surface energy partition during August. Although the optimization period is the first 10 days of August, the soil temperatures at the surface and at a depth of 5 cm are perfectly reproduced in the following days, as shown in Fig. 6. Accordingly, the net radiation and soil heat fluxes are also well reproduced, as shown in Fig. 7a and 7b. The comparisons of the sensible heat and the latent heat are shown in Fig. 7c and 7d. The simulated sensible heat flux H_{opt} agrees well with the measurement H_{obs}, while the simulated latent heat flux lE_{opt} is much higher than the observation lE_{obs} in general. The mean measured sensible heat flux during 10LT–16LT is 69.5 Wm^{-2}, close to the optimal flux (81.1 Wm^{-2}); while the mean observed latent heat flux is 118.5 Wm^{-2}, only about half the optimal flux (220.2 Wm^{-2}). To evaluate the effect of the large discrepancy in the latent heat, we use the optimal latent heat flux instead of the measured flux to calculate the residual energy, i.e.,

$$E_{ropt} = R_{nobs} - H_{obs} - lE_{opt} - G_0. \quad (25)$$

The residual energy from Eq. (25) is shown in Fig. 7e. It shows that the residual energy mostly falls in the range of ± 50 Wm^{-2} and seldom excesses 100 Wm^{-2}. The mean residual energy during 10LT–16LT from Eq. (25) is only 12.1 Wm^{-2}, while the observed mean value is as high as 113.8 Wm^{-2}. The gap therefore suggests that the error in the latent heat flux may be the main factor responsible for the low energy closure ratio mentioned in Section 3.2.

5. Sensitivity studies on energy partition

There are some uncertainties that may affect the optimization of the model parameters and thus the simulation of the energy partition in Section 4. Their effects are clarified in the following case studies.

5.1 Optimization duration

In Case 1, the data for the first 10 days of August are used for the parameter optimization. It is not clear whether the optimization duration is sufficient or whether the optimal values are sensitive to the optimization duration, so these parameters are optimized again based on the data for the first 20 days (Case 2a) or the whole month (Case 2b). The optimized values are shown in Table 3. The results indicate that the values except for the coefficients

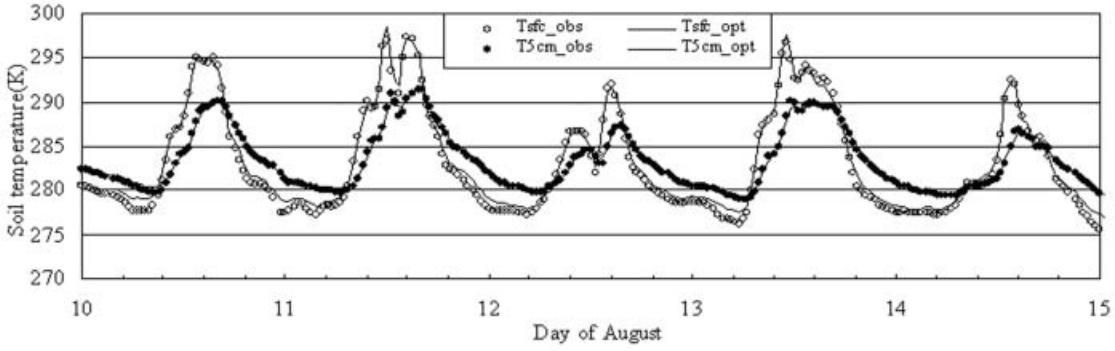

Fig. 6. Comparison of the soil temperatures between observations and simulations with optimal parameters in Case 1.

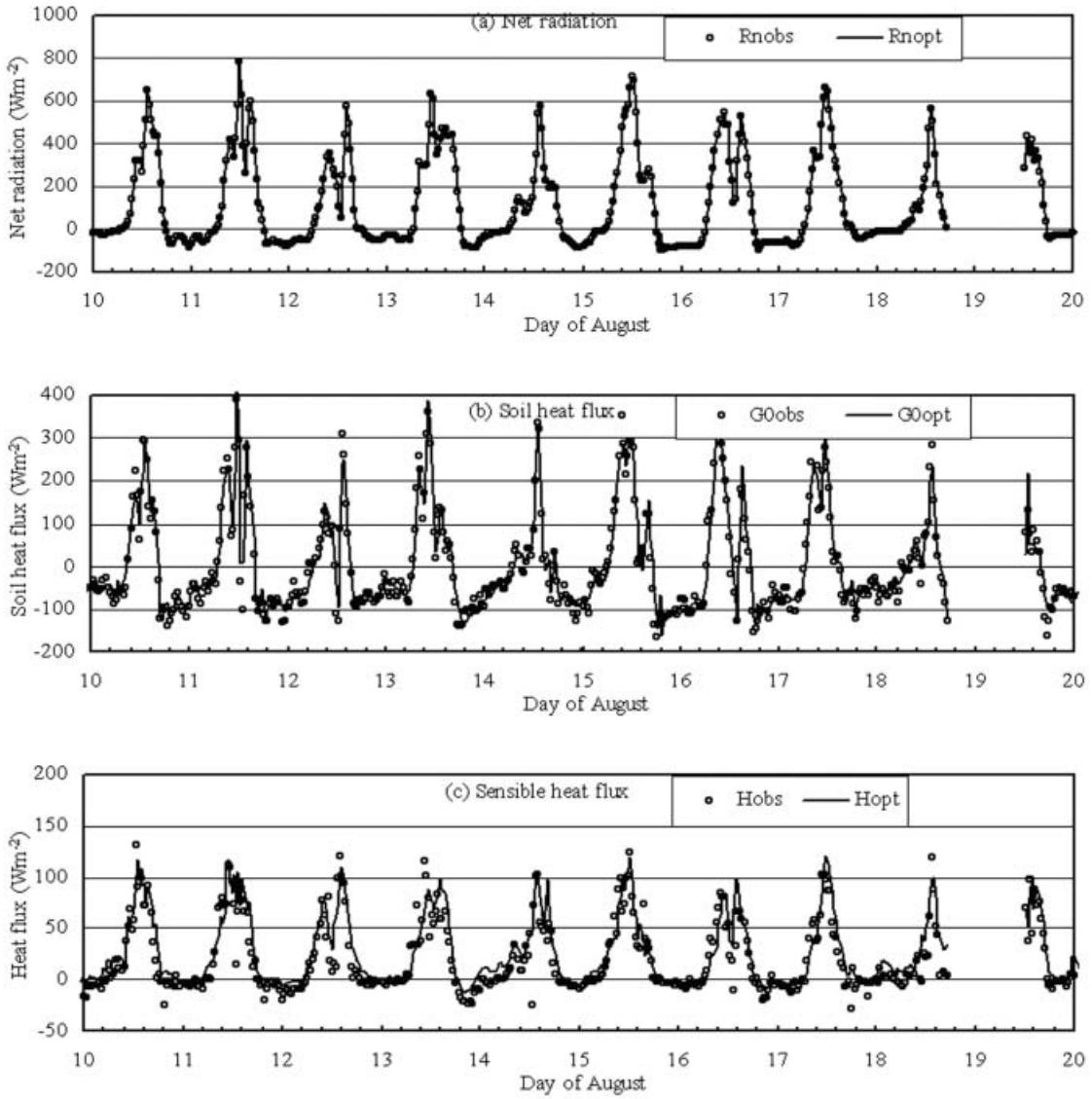

Fig. 7. Comparison of the energy partition between observations and simulations in Case 1.

c_1 and c_2, are not sensitive to the optimization duration. Noting that the soil surface resistance R_s is mainly determined by the difference $c_1 - c_2$ for the wet surface, so the difference in R_s between these cases can be neglected, and the energy partition changes little (not shown). Therefore, a duration of 10 days is sufficiently long for parameter optimization.

5.2 Soil thermal conductivity

The soil thermal conductivity λ_s is derived from the soil temperature and the soil heat flux. The latter has a 10% uncertainty, as mentioned in Section 3, so the parameters are optimized again with the condition that λ_s increases 10% in one case (Case 3a) or decreases 10% in another case (Case 3b). The optimized values are also shown in Table 3. Figures 8a and 8b give the sensible heat flux, and latent heat flux simulated with these parameters. During 10LT–16LT in the daytime, the mean difference between Case 1 and Case 3a is 2.2 $\mathrm{Wm^{-2}}$ in the sensible heat flux and 2.7 $\mathrm{Wm^{-2}}$ in the latent heat flux, and that between Case 1

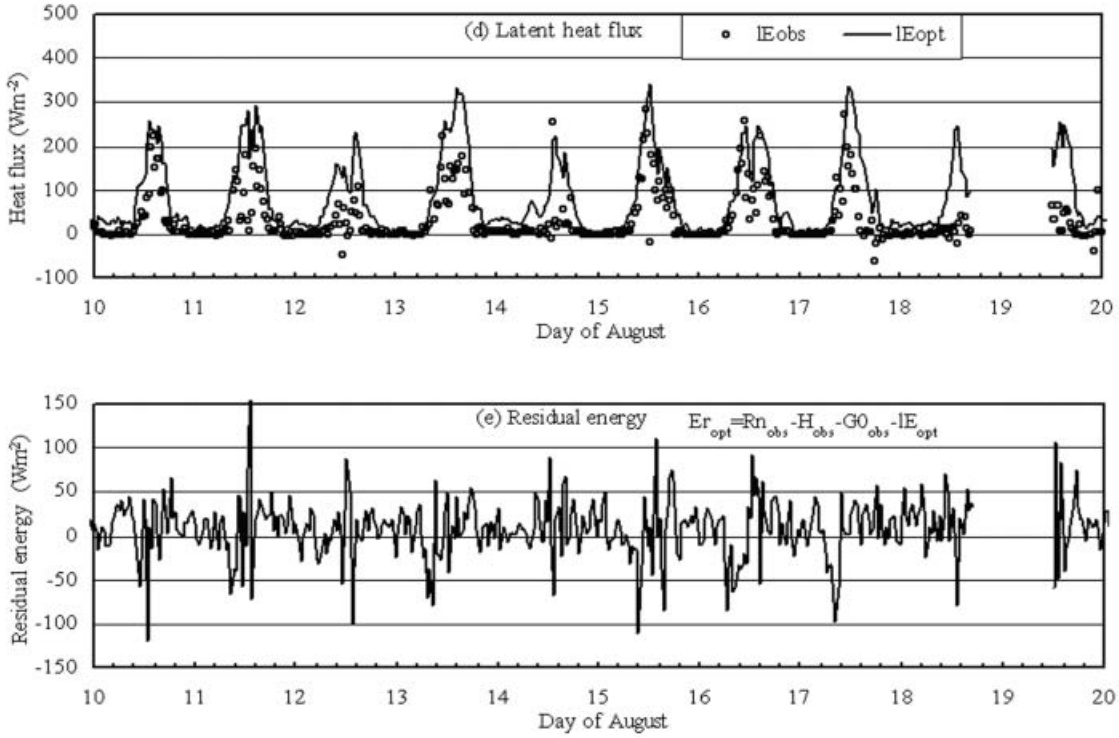

Fig. 7 (continued)

and Case 3b is 10.4 Wm^{-2} in the sensible heat flux and 7.8 Wm^{-2} in the latent heat flux. The uncertainty is no more than 12% in the sensible heat flux and 5% in the latent heat flux, which is close to or less than the uncertainty in the soil heat flux. That is, the model does not amplify the uncertainty in the soil heat flux.

5.3 Stability function

On the Tibetan Plateau, due to the strong solar radiation, the air-surface temperature difference can reach more than 30 K in the dry season and 15 K in the wet season, so the surface layer can be highly unstable in the daytime. The Högström's (1996) stability functions are suggested to be applicable only for $z/L > -3$. Kader and Yaglom (1990) reasoned that the atmospheric surface layer can be subdivided into three sublayers, namely, the dynamic sublayer, the dynamic-convective sublayer, and the free convection sublayer. In each they propose a simple power law to describe the mean velocity and temperature profiles. Because their functions cover only certain ranges of stability, Brutsaert (1999) fitted their data and gave the following functions:

$$\phi_m = (a_1 + a_2(z/L)^{1/3})/(a_1 + z/L), \tag{26a}$$

$$\phi_h = (a_3 + a_4 y^n)/(a_3 + y^n), \tag{26b}$$

where $a_1 = 0.33$, $a_2 = 0.41$, $a_3 = 0.33$, $a_4 = 0.057$, and $n = 0.78$.

Since we applied Högström's (1996) relationship to all unstable conditions, without identifying strong instabilities, it is necessary to show how different fluxes may be caused if strong instabilities are considered in the profile functions. We therefore calculate the energy partition using Eq. (26) and the optimal parameters in Case 1. Figure 9 shows the flux difference caused by Högström's (1996) and Brutsaert's (1999) stability functions. The turbulent fluxes calculated with the latter are lower than those with the former. But their difference in sensible heat is no more than 12.7 Wm^{-2}, and that of the latent heat flux is no more than 27.7 Wm^{-2}. During 10LT–16LT in the daytime, the mean difference in sensible heat is 5.1 Wm^{-2}, or 6.5%; and in latent heat

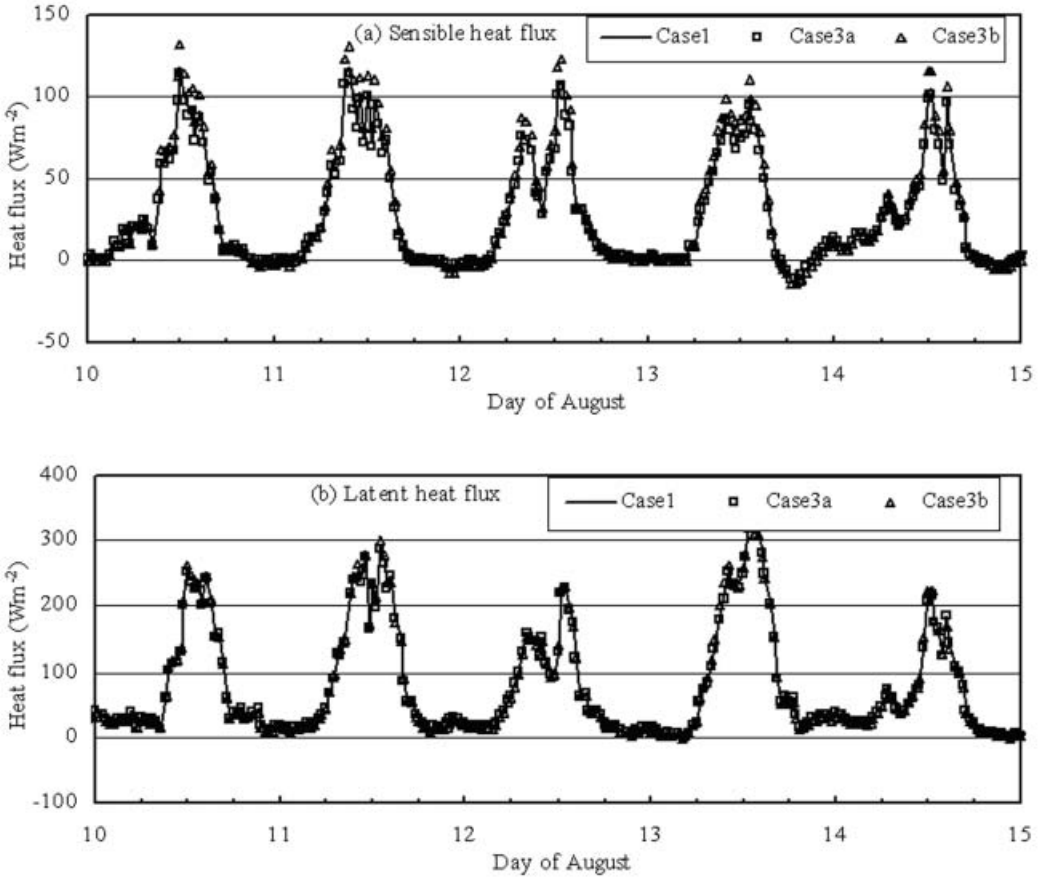

Fig. 8. Comparison of the energy flux between Case 1, Case 3a and Case 3b: (a) sensible heat (b) latent heat.

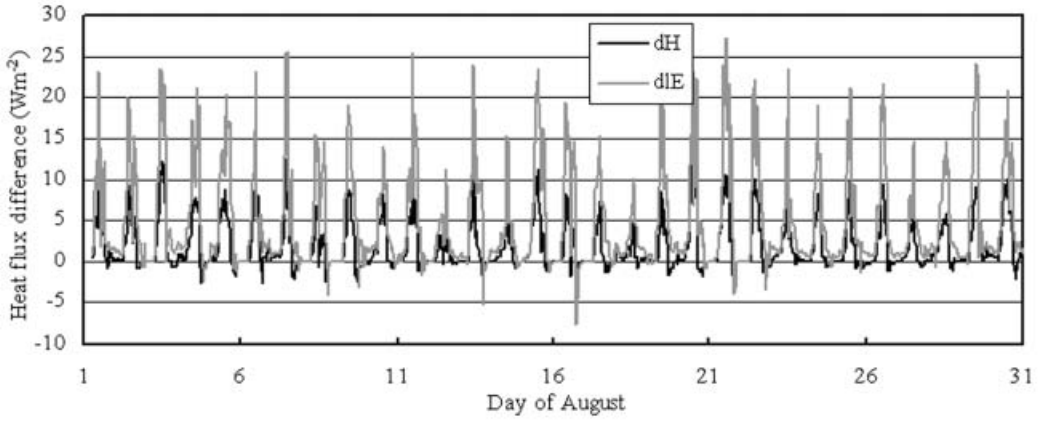

Fig. 9. Flux difference due to the different stability functions of Högström (1996) and Brutsaert (1999) (the former minus the latter). dH: sensible heat flux difference; dlE: latent heat flux difference.

is 11.6 Wm^{-2}, or 5.4%, so selecting a different stability function does not significantly change the energy partition. Furthermore, if we optimize the parameters using Eq. (26), the resulting energy partition is very close to that using Eq. (16), as in Case 1.

In summary, the energy partition obtained in Section 4 is not sensitive to the optimization duration, the error in soil thermal conductivity, nor the choice of stability functions.

6. Vegetation effect on energy partition

Although the plateau grasses are sparse and short, the sensible heat and latent heat are essentially transferred from both the vegetation and the ground surface. However, this dual-source process is approximated by the single-source model in Section 4. To justify the simplification, we need to demonstrate that the energy partition between the sensible heat and the latent heat is not sensitive to the short and sparse vegetation on the wet plateau surface. This section therefore uses the dual-source model SiB2 to illustrate the sensitivities of vegetation coverage and leaf area index on the energy partition. Due to the complex subsurface soil water flow, we will not involve its modeling. Instead, the measured soil water content is supplied as input data, as done in Section 4 and 5, so that we can focus on the energy partition analysis.

Based on the in situ vegetation conditions, the following SiB2 parameters are determined: the canopy top height $z_2 = 0.05$ m; the canopy base height $z_1 = 0.01$ m; the canopy inflection height $z_c = 0.03$ m; the leaf width $l_w = 0.004$ m; the leaf length $l_l = 0.04$ m; the green leaf fraction $N = 0.95$; the ground aerodynamic roughness length $z_s = 0.0013$ m; the leaf angle distribution factor $\chi_L = -0.3$; the air density 0.71 kgm^{-3}; the reference height $z_{m1} = 14.0$ m for wind speed; and, $z_{m2} = 13.75$ m for the temperature and humidity. These parameters together with the vegetation coverage V_c and the leaf area index LAI can be used to determine the aerodynamic parameters in SiB2. The vegetation optical and physiological properties are specified according to the SiB2 vegetation type 6 (grass) (see Table 5 in Sellers et al. 1996b).

The soil hydraulic properties are given by the experimental results shown in Table 2. The derived soil thermal conductivity and optimized soil resistance for evaporation in Section 4 are used. The soil reflectance is 0.11 for visible light and 0.18 for near infrared light, and is calibrated from the measured downward and upward shortwave. The soil wetness in each layer is defined as $(\theta - \theta_{rsd})/(\theta_{sat} - \theta_{rsd})$ instead of θ/θ_{sat}.

The root depth $D_r = 0.1$ m was observed, while the surface soil depth $D_1 = 0.04$ m and total soil depth $D_T = 1.0$ m are assumed. The value of D_T is not important, since the soil water content in all of the layers is supplied from observations.

Although there are some uncertainties in many of the vegetation parameters, we focus mainly on the sensitivity of the surface energy partition to vegetation coverage and LAI because the energy partition is significantly affected by these two parameters. Therefore, four cases are designed: in Case A, $LAI = 0.2$ and $V_c = 0.2$; in Case B, $LAI = 0.4$ and $V_c = 0.2$; in Case C, $LAI = 0.4$ and $V_c = 0.4$; and in Case D, $LAI = 0.6$ and $V_c = 0.4$. In all of the cases, the observations at Anduo are used for model initialization and forcing data. Since all of the conditions except V_c and LAI are identical in all of the cases, the difference in the simulated temperature and energy partition would show the vegetation effect.

At first, the simulated temperature difference $T_g - T_c$ and $T_g - T_{sfc}$, and the simulated and observed radiative temperatures (converted from upward longwave) T_{sfc} are shown in Fig. 10a–10c for the four cases. T_g is the ground temperature, and T_c is the canopy temperature. Figure 10a shows that the temperature difference $|T_g - T_c|$ decreases with increasing leaf area index. The maximum difference is 6.2 K in Case A and 4.8 K in Case D. However, the temperature difference $|T_g - T_{sfc}|$ increases with increasing leaf area index, but is much smaller than the difference $|T_{sfc} - T_c|$. The maximum $|T_g - T_{sfc}|$ is 0.7 K in Case A and 1.5 K in Case D. In the extreme case of $LAI = 0.0$, this temperature difference would vanish. In other words, it is reasonable to approximate $T_g \approx T_{sfc}$ for the plateau vegetation covered surface, as done in Section 3. Figure 10c shows that the surface radiative temperature in all of the cases agrees with the observed very well. This means that the upward longwave radiation, and thus the net radiation, is

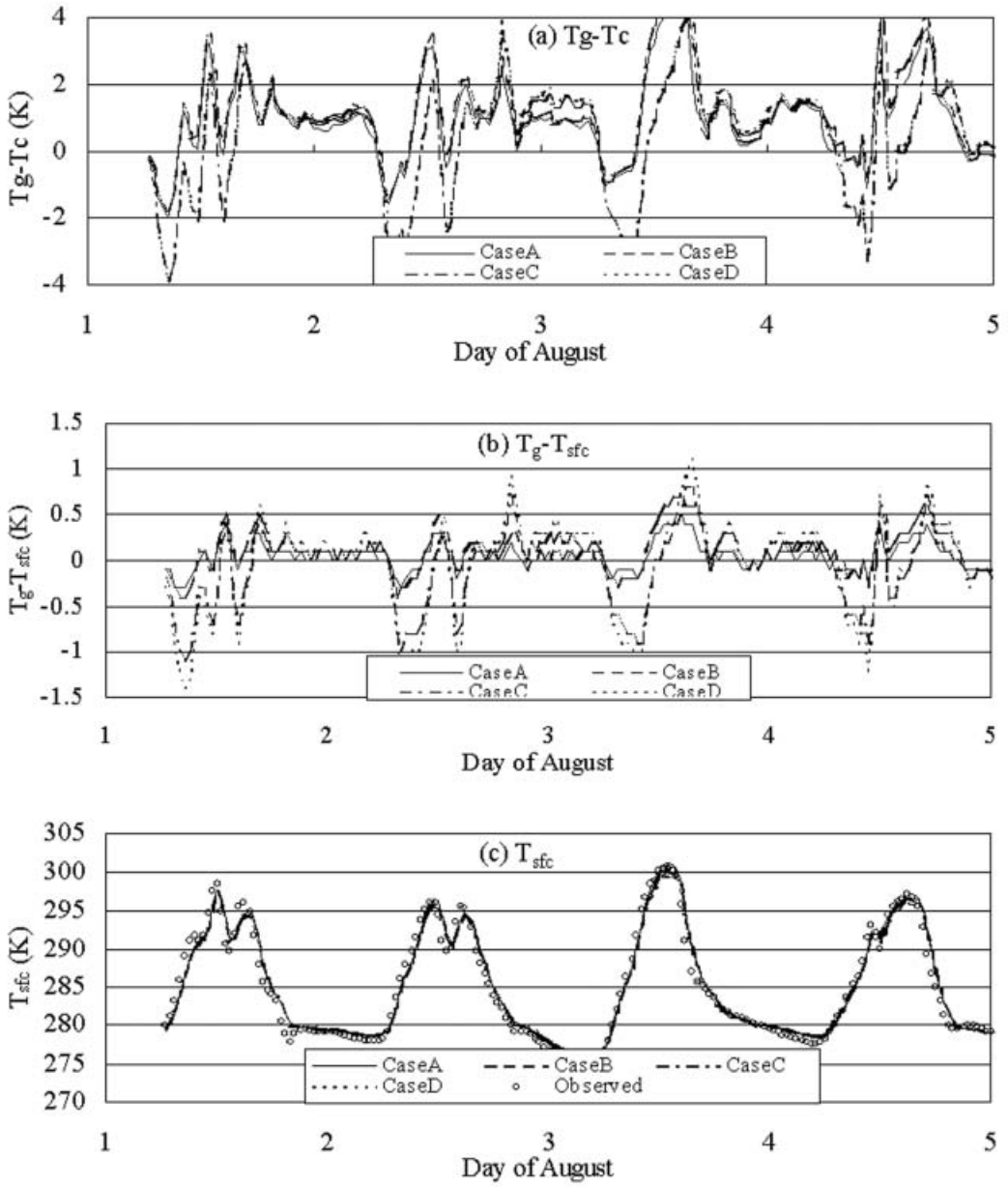

Fig. 10. Comparison between the simulated canopy temperature, ground temperature and surface radiative temperature.

not sensitive to the vegetation coverage nor the leaf area index.

Secondly, the energy partition between the vegetation and the ground is shown in Fig. 11a–11c for sensible heat and in Fig. 12a–12c for latent heat. The sensible heat flux from the vegetation in Fig. 11a is comparable to that from the ground in Fig. 11b, because the heat transfer resistance from the ground to the canopy air space is comparable to that from the leaf surface to the canopy air space. However, the latent heat flux from the vegetation in Fig. 12a is much less than that from the ground in Fig. 12b because the stomatal resistance for transpiration is much higher than the soil resistance for evaporation in the plateau climatic conditions (low temperature, low humidity, low CO2 concentration, and wet surface). These fig-

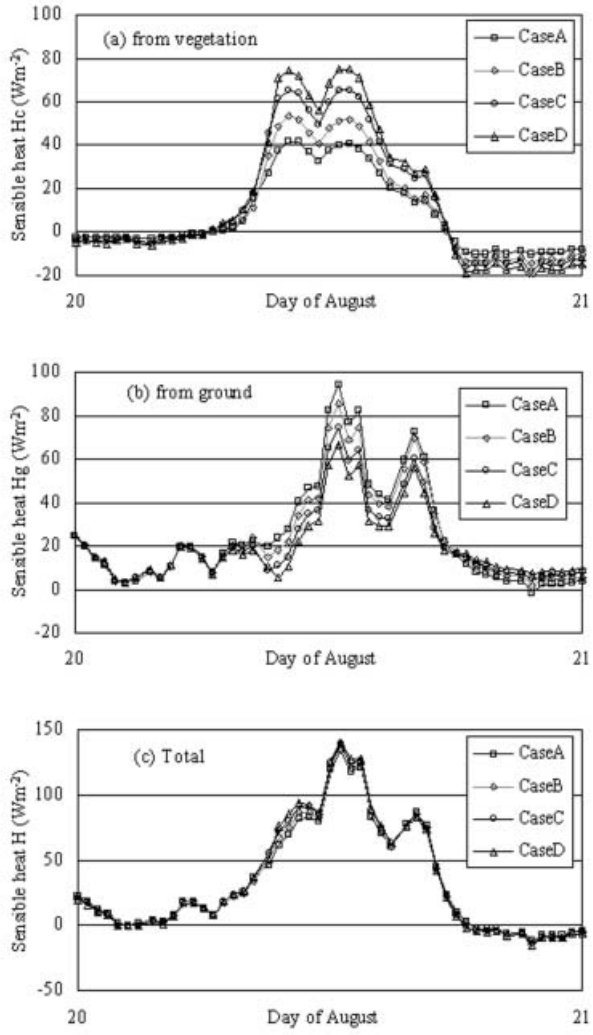

Fig. 11. Simulated sensible heat partition between the vegetation and the ground for August 20.

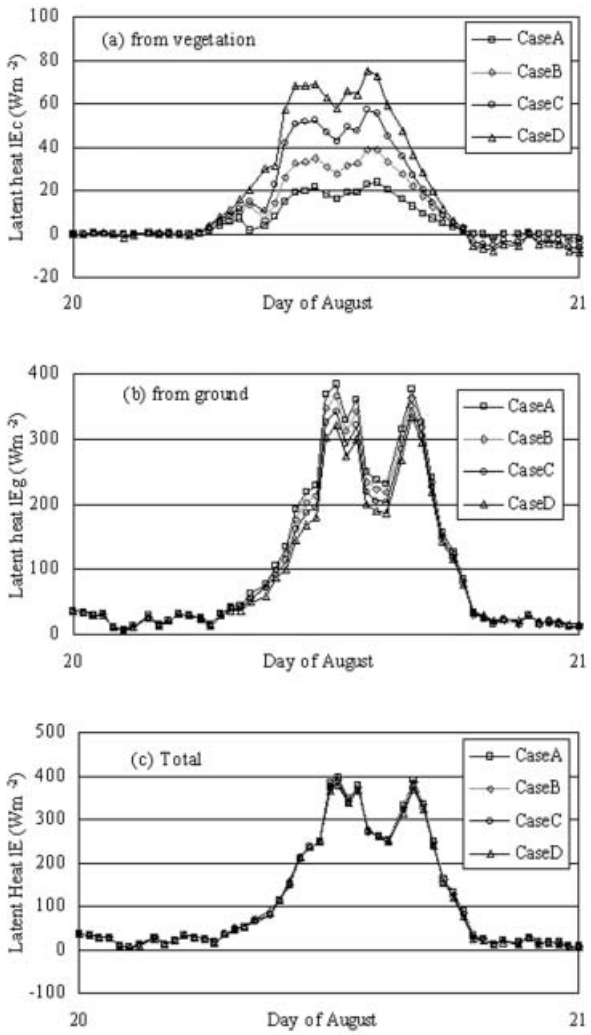

Fig. 12. Simulated latent heat partition between the vegetation and the ground for August 20.

ures also indicate that increasing the leaf area index and the vegetation coverage would result in more heat fluxes from the vegetation while less from the ground. The vegetation therefore plays an apparent role in the energy partition between the vegetation and the ground. From the viewpoint of energy source, the energy partition is essentially a dual-source process. However, Fig. 11c and 12c illustrate that the sum of the heat fluxes from the vegetation and the ground is almost the same in all of the cases, which means that the energy partition between the total sensible heat and the total latent heat is insensitive to the leaf area index and the vegetation coverage. Therefore, from the viewpoint of land-atmosphere interactions, the energy partition is essentially a single-source process, which justifies the simple energy partition model used in Sections 4 and 5.

Finally, the comparisons of the energy partition between the observations, the optimization in Section 4, and the SiB2 simulation in Case C are shown in Fig. 13a–13c for sensible heat, latent heat, and soil heat flux, respectively. These figures show that the simulated energy partitions from SiB2 and from the simple en-

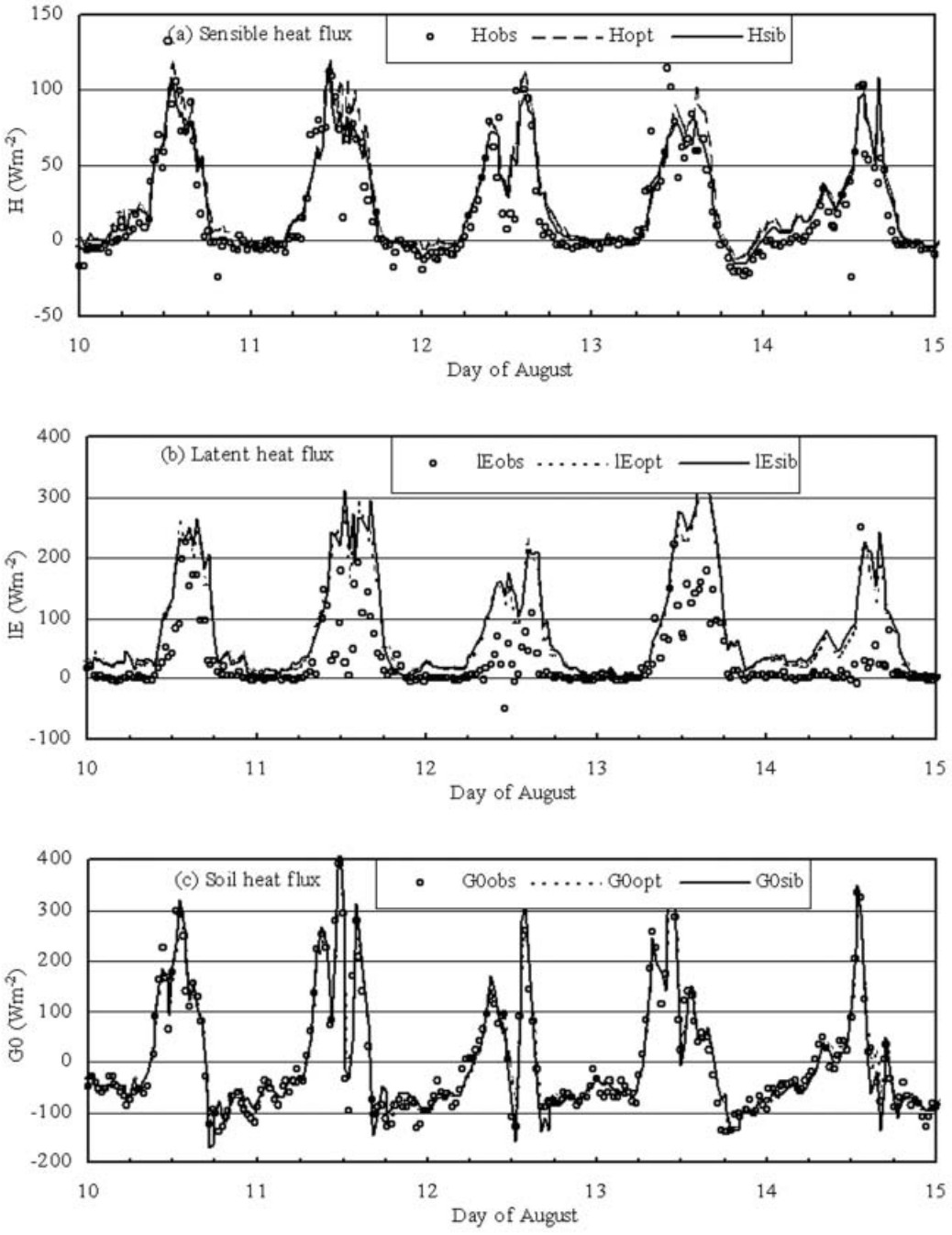

Fig. 13. Comparison of the energy partition between the observation, optimization and SiB2 simulation.

ergy partition model are very similar, which, again, shows that the single-source model is suitable for the plateau short vegetation and the meteorological conditions. If the observed latent heat flux in the energy budget equation is replaced with the SiB2 simulation, the mean residual energy during 10LT–16LT is as low as 5.0 Wm^{-2}. This suggests a similar conclusion,

that the sensible heat flux was measured correctly, while the latent heat flux was undermeasured.

7. Discussion on energy closure problem

The above analysis suggests that the measured sensible heat flux is reasonable, while the latent heat flux may be significantly undermeasured by the eddy-correlation technique. We suggest that the latter plays a major role in the energy closure problem. However, it is not clear why such a situation occurred at this flat and open site. The following gives a brief discussion from both instrumentation and physical points of view.

Figure 5b shows that the energy closure ratio before August 23 is obviously less than after August 23. The mean closure ratio is as low as 0.57 in the first 23 days. Afterwards, the mean ratio reaches 0.79, and even higher than 0.9 in three days (26, 29 and 30). This sudden change resulted from the replacement of the infrared (IR) source of the hygrometer on August 23. At the Anduo site, the IR hygrometer was used to detect both high frequency and low frequency fluctuations of specific humidity, and a capacity-type hygrometer was used to detect the low frequency fluctuations. After filtering the high-frequency fluctuations, the specific humidity measured by the IR hygrometer was poorly correlated with that measured by the capacity-type hygrometer, because the ray of the IR hygrometer was weakened by the precipitation from July to August (Tanaka et al. 2001b). The correlation was lower than 0.7 in the first 23 days of August, which means a low quality of the turbulence data. After the bulb of the IR source was replaced on August 23, the correlation improved to more than 0.8, and to even more than 0.9 on some days. The higher quality turbulence data leads to a higher latent heat flux, and thus a higher closure ratio. The result therefore suggests that this measurement error in humidity fluctuations plays a key role in the closure problem.

The under-measurement of the latent heat is also associated with rainfall events. To illustrate this point, Fig. 14 shows the relationship between the accumulated rainfall amount during 06LT–16LT, and the energy closure ratio during 10LT–16LT. The data before and after August 23 are marked by different symbols.

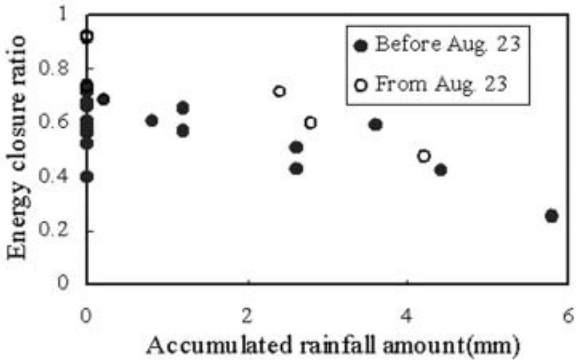

Fig. 14. Relation between accumulated rainfall amount during 06–16LT and the energy closure ratio during 10–16LT at Anduo.

Fig. 14 clearly shows that low closure ratios usually occurred during rainy daytimes, while high closure ratios occurred during rain-free daytime, regardless of the replacement of the IR source on August 23. As shown in Fig. 7c and Fig. 15, the rainfall events have a small effect on the sensible heat measurement, but its effect on latent heat measurements is obvious. The result indicates that the sensor of the IR hygrometer does not work correctly during and several hours after precipitation, because raindrops may absorb infrared light when attaching to the lens of the hygrometer sensor, and water vapor may subsequently intrude into the inside of the sensor (Tamagawa 1999). Therefore, this simple optical hygrometer is not very suitable for field measurements in rainy conditions, and frequent calibration is indispensable. On the other hand, Fig. 15 shows that both the measured sensible heat and the latent heat are comparable to the optimized heats during rain-free daytime (Days 26, 29, 30). This, in turn, demonstrates that the simulated results are reliable.

From the viewpoint of physical processes, horizontal advection may also play a different role in sensible heat and latent heat transport. At the Anduo site, the field measurements were not designed to address the problem of horizontal advection. However, the presence of horizontal advection may be inferred from the testing of the flux-variance similarity relationships for heat and water vapor. Kim et al. (2001) thus analyzed the turbulence data at

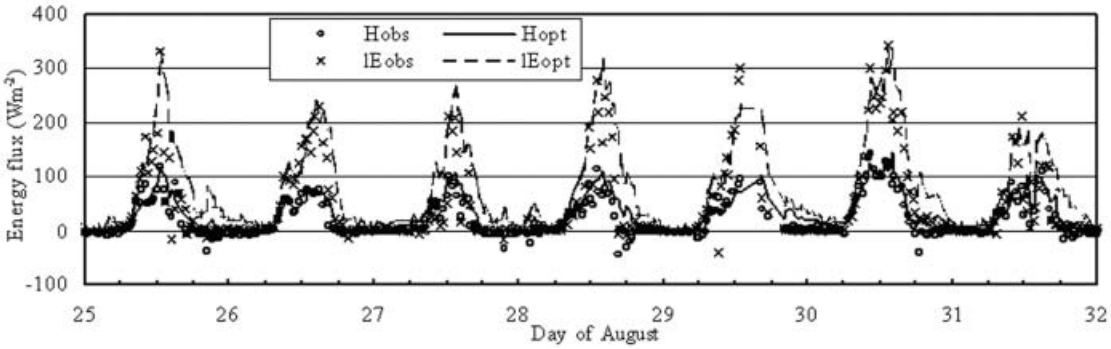

Fig. 15. Comparison between the observed and optimized heat fluxes during 25–31, August.

the GAME/Tibet Naqu site where the surface characteristics and energy closure problem are similar to the Anduo site. The similarity constant for σ_T/T_* over the plateau prairie is about 0.93–0.98, close to the values obtained from homogeneous sites reported in the literature (Wyngaard et al. 1971; Albertson et al. 1995). The constant for σ_q/q_* is about 1.1–1.5, which is larger than the constant for σ_T/T_*. Since the two constants should be identical for imaginary homogeneous surfaces, this difference suggests that the sources and sinks of heat and water vapor on the plateau surface may be different. These surfaces may be homogeneous for the sinks and sources of heat while heterogeneous for water vapor. Similar phenomena were reported in earlier studies (Katul et al. 1995; Andreas et al. 1998). Therefore, the horizontal advection of sensible heat may be neglected, while that of latent heat might be important. On the other hand, Mahrt (1998) pointed out that the surface heterogeneity may cause tower flux errors to increase with decreasing wind speed; in other words, the energy closure ratio may increase with increasing wind speed. We thus investigated the relationship between the energy closure ratio and the wind speed at the Anduo site, but no clear trend is found, so it is still difficult to quantitatively evaluate the effect of the horizontal advection of latent heat on the energy closure.

Besides horizontal advection, two other processes that may affect the measurements of the sensible heat flux and the latent heat flux are addressed below.

(1) Energy storage in the air and vegetation. This term has been shown to be important for the energy closure at forest sites (Lee and Black 1993; Fitzjarrald and Moore 1994). At the Anduo site, the flux tower is 2.85 m above the ground, and the vegetation heat capacity is very low. We estimate that the hourly mean energy storage is usually much less than 10 Wm^{-2}, and that the daily mean is close to zero. Therefore, this term plays only a negligible role in the plateau energy closure problem.

(2) Transport by mean vertical velocity. The mean vertical velocity may result from stationary motion (Mahrt 1998), convection, synoptic scale subsidence, and local circulations (Lee 1998). This vertical transport by mean velocity is given by $\rho\overline{w}_r(\bar{c}_r - \langle\bar{c}\rangle)$ (Lee 1998). Here, $\overline{w}_r$ and $\bar{c}_r$ are the mean wind speed and concentration at the reference level, and $\langle\bar{c}\rangle$ is the averaged concentration from the ground to the reference level. If we ignore the stability effect on temperature and the humidity profile, the ratio of the advective transport to the turbulent transport can be simplified to $\overline{w}_r/ku_*$. Because $\overline{w}_r$ increases with height, the ratio would increase with height. In typical convergence cases like $\partial u/\partial x = 0.001\ \mathrm{s}^{-1}$, $\overline{w}_r$ will be 0.285 cms^{-1} at the measurement level (2.85 m) of our site. Given the plateau typical value of $u_* = 0.15$ ms^{-1}, the ratio is estimated to be about 5%. In the case of divergence, however, $\overline{w}_r$ is much less than in the case of convergence, and thus the ratio is much less. Lee (1998) pointed out that the probability of the meteorological tower instruments being influenced by the descending motion was much higher than by ascending motion. Therefore, we could speculate that the vertical transport by the mean velocity might occasionally cause several percentages of the

energy imbalance, but it would be unimportant in general. This is only a qualitative estimation. An experiment is being implemented at a plateau site, which includes two sets of turbulence measuring systems mounted at two different levels, respectively. This experiment will provide the data required for a quantitative evaluation of the vertical advection.

8. Summary

Based on field observations in 1998 and recent laboratory experiment results, this study analyzed the surface energy budget at a GAME plateau site during the wet season. With measured sensible heat, latent heat, net radiation, and reliably derived surface soil heat flux, we found that the mean energy closure ratio in the daytime was as low as 0.64 in August, an occurrence that was not expected for the flat plateau surface.

Based on our investigation, we conclude that the measured sensible heat flux is reliable while the latent heat flux is under-measured. The latter is one major factor responsible for the low energy closure ratio at the site of interest. This measurement error is caused by two instrument problems. One is that the infrared power of the hygrometer sensor could be weakened by precipitation. The other is that raindrops may attach to the lens of the hygrometer sensor and absorb infrared light, and water vapor may subsequently intrude into the inside of the sensor. Therefore, the frequent in-field calibration of this type of optical hygrometer is indispensable for long-term field experiments during the rainy season. Another factor that may affect the energy closure is the horizontal advection of the latent heat, but it is still difficult to evaluate this term quantitatively. Other factors such as the heat storage in the air and in the vegetation, and the vertical advective transport might not cause a significant energy closure problem.

To simulate the surface energy budget on the plateau surface, we introduced a single-source surface energy partition model to approximate the surface energy budget processes, which are essentially dual-source from the viewpoint of heat and water vapor sources. This simplification is supported by sensitivity studies using a dual-source model, which show that the energy partition between the sensible heat and the latent heat is insensitive to the leaf area index, and the vegetation coverage for the plateau sparse and short prairie. Compared to a dual-source model, the single-source model has a small number of model parameters, and thus can be calibrated more easily. The model is validated by the good agreement between measured and simulated heat fluxes on days with high energy closure ratios. Therefore, the single-source simplification is applicable to the heat transfer on the plateau sparse-vegetation surface, and the energy partition can be estimated properly by using this model, even when the in situ measurements could not be trusted. From the viewpoint of the land surface contribution to the atmosphere, this single-source concept would greatly contribute to further studies on the plateau land-atmosphere interactions. An important application is to develop a unique land surface model for the plateau surface, no matter if it is a bare soil surface in the dry season, or a vegetation-covered surface in the wet season.

Acknowledgement

The data used in this paper were obtained through the GAME/Tibet project. The authors would like to acknowledge all of the scientists involved in the field work at Anduo of the GAME/Tibet project. We are grateful to the two reviewers and Dr. Tsutomu Watanabe who provided invaluable comments and suggestions for improving the quality of the paper. Great thanks also go to Dr. Kenji Tanaka, Dr. Jieming Wang, Dr. Joon Kim, and Dr. Min Li, for their valuable discussions.

References

Albertson, J.D., M.B. Parlange, G.G. Katul, C.-R. Chu, and H. Stricker, 1995: Sensible heat flux from arid regions: A simple flux-variance method, *Water Resour. Res.*, **31**, 969–973.

Andreas, E., R.J. Hill, J.R. Gosz, D.I. Moore, W.D. Otto, and A.D. Sarma, 1998: Statistics of surface-layer turbulence over terrain with metre-scale heterogeneity, *Boundary-Layer Meteor.*, **86**, 379–408.

Asrar, G., M. Fuchs, E.T. Kanemasu, and J.L. Hatfield, 1984: Estimating absorbed photosynthetic radiation and leaf area index from spectral reflectance in wheat, *Agron. J.*, **76**, 300–306.

Bian, L., Z. Gao, X. Xu, Y. Cheng, 2002: Measurements of turbulence transfer in the near-surface layer over the southeastern Tibetan Plateau., *Boundary-Layer Meteor.*, **102**, 281–300.

Brutsaert, W., 1999: Aspects of bulk atmospheric boundary layer similarity under free-convective conditions, *Rev. Geophy.*, **37**, 439–451.

Dougherty, D.E. and R.A. Marryott, 1991: Optimal groundwater management, Part I: Simulated annealing, *Water Resour. Res.*, **27**, 2493–2508.

Fitzjarrald, D.R. and K.E. Moore, 1994: Growing season boundary layer climate and surface exchanges in a subarctic lichen woodland, *J. Geophys. Res.*, **99**, 1899–1917.

Högström, U.L.F., 1996: Review of some basic characteristics of the atmospheric surface layer, *Boundary-Layer Meteor.*, **78**, 215–246.

Ishikawa, H., T. Hayashi, K. Tanaka, O. Tsukamoto, H. Fudeyasu, I. Tamagawa, J. Asanuma, Y. Qi, J. Wang, Y. Ma, Z. Hu, and H. Gao, 1999: Summary and the preliminary results of PBL observation, *Proceedings of the 1st international workshop on GAME-Tibet*, Xian, China, 11–13, January, 1999, 69–72.

Jacobsen, O.H. and P. Schjønning, 1993: A laboratory calibration of time domain reflectometry for soil water measurement including effects of bulk density and texture, *J. Hydrol.*, **151**, 147–157.

Kader, B.A. and A.M. Yaglom, 1990: Mean fields and fluctuation moments in unstably stratified turbulent boundary layers, *J. Fluid Mech.*, **212**, 637–662.

Katul, G., S.M. Goltz, C.-I. Hsieh, Y. Cheng, F. Mowry, and J. Sigmon, 1995: Estimation of surface heat and momentum fluxes using the flux-variance method above uniform and non-uniform terrain., *Boundary-Layer Meteor.*, **74**, 237–260.

Kim, J., J. Hong, S.-Y. Hong, T. Choi, N. Chae, Z. Gao, J. Asanuma, I. Takayabu, M. Tsujimura, O. Tsukamato, H. Ishikawa, N. Yamazaki, J. Wang, T. Koike, T. Yasunari, 2001: On measuring and modeling surface energy partitioning in a Tibetan Prairie during GAME-IOP 1998, *Proceedings of the fifth international study conference on GEWEX in Asia and GAME*, Nagoya, Japan, 3–5, October, 2001, 19–25.

Kirkpatrick, S., C.D. Jr. Gelatt, M.P. Vecchi, 1983: Optimization by simulated annealing, *Science*, **220**(4598), 671–680.

Kondo, S., 1994: *Hydrometeorology: Water and Energy Budget on Ground Surfaces* (in Japanese), Asakura Publishing House, Japan, 194–198, 348pp.

Lamaud, E., J. Ogee, Y. Brunet, and P. Berbigier, 2001: Validation of eddy flux measurements above the understorey of a pine forest, *Agr. For. Meteorol.*, **106**(3), 187–203.

Lee, X., 1998: On micrometeorological observations of surface-air exchange over tall vegetation, *Agr. For. Meteorol.*, **91**, 39–49.

——— and T.A. Black, 1993: Atmospheric turbulence within and above a douglas-fir stand. Part II: Eddy fluxes of sensible heat and water vapour, *Boundary-Layer Meteor.*, **64**, 369–389.

Mahrt, L., 1998: Flux sampling errors for aircraft and towers, *J. Atmos. Oceanic Technol.*, **15**, 416–428.

McCaughey, J.H., P.M. Lafleur, D.W. Joiner, P.A. Bartlett, A.M. Costello, D.E. Jelinski, and M.G. Ryan, 1997: Magnitudes and seasonal patterns of energy, water, and carbon exchanges at a boreal young jack pine forest in the BOREAS northern study area, *J. Geophys. Res.*, **102**(D24), 28997–29007.

Miyazaki, S., O. Tsukamoto, I. Kaihotsu, T. Miyamoto, and T. Yasunari, 2000: The energy imbalances observed in Tibetan Plateau and Mongolian Plateau, *The 2nd session of international workshop on TIPEX-GAME/Tibet*, 20–22, July, 2000, Kunming, China, 1–3.

Nie, D., E.T. Kanemasu, L.J. Fritschen, H.L. Weaver, E.A. Smith, S.B. Verma, R.T. Field, W.P. Kustas, and J.B. Stewart, 1992: An intercomparison of surface-energy flux measurement systems used during FIFE 1987, *J. Geophys. Res.*, **97**(D17), 18715–18724.

Philip, J.R., 1961: The theory of heat flux meters, *J. Geophys. Res.*, **66**, 571–579.

Roth, C.H., M.A. Malicki, R. Plagge, 1992: Empirical-evaluation of the relationship between soil dielectric-constant and volumetric water-content as the basis for calibration soil-moisture measurements by TDR, *J. Soil Sci.*, **43**(1), 1–13.

Sellers, P.J., D.A. Randall, G.J. Collatz, J.A. Berry, C.B. Field, D.A. Dazlich, C. Zhang, G.D. Collelo, and L. Bounoua, 1996a: A revised land surface parameterization (SiB2) for atmospheric GCMs. Part I: Model formulation, *J. Climate*, **9**, 676–705.

———, S.O. Los, C.J. Tucker, C.O. Justice, D.A. Dazlich, G.J. Collatz, and D.A. Randall, 1996b: A revised land surface parameterization (SiB2) for atmospheric GCMs. Part II: The generation of global fields of terrestrial biophysical parameters from satellite data, *J. Climate*, **9**, 706–737.

Szu, H. and R. Hartley, 1987: Fast simulated annealing, *Physics Letters A*, **122**, 157–162.

Tamagawa, I., 1999: Considerations on the eddy correlation method using sonic anemometer-thermometer and infrared hygrometer (in Japanese), *J. Japan Soc. Hydrol. & Water Resour.*, **12**(2), 130–198.

Tanaka, K., H. Ishikawa, T. Hayashi, I. Tamagawa, and Y. Ma, 2001a: Surface energy budget at Amdo on the Tibetan Plateau using GAME/Tibet IOP98 data, *J. Meteor. Soc. Japan*, **79**(1B), 505–517.

———, ———, and I. Tamagawa, 2001b: Surface energy budget in the eastern Tibetan Plateau during GAME-Tibet IOP 1998, *Proceedings of the fifth international study conference on GEWEX in Asia and GAME*, Nagoya, Japan, 3–5, October, 2001, 87–90.

Twine, T.E., W.P. Kustas, J.M. Norman, D.R. Cook, P.R. Houser, T.P. Meyers, J.H. Prueger, P.J. Starks, and M.L. Wesely, 2000: Correcting eddy-covariance flux underestimates over a grassland, *Agr. For. Meteorol.*, **103**(3), 279–300.

Wang, J., J. Kim, Y. Liou, Z. Gao, Y. Yan, T. Choi, and H. Lee, 1999: Energy balance analysis and one-dimensional simulation of land surface processes in a short-grass site of central Tibetan Plateau. *Proceeding of the 1st international workshop on GAME-Tibet*, Xian, China, 11–13, January, 1999, 73–76.

Webb, E.K., G.I. Pearman, and R. Leuning, 1980: Correction of flux measurement for density effects due to heat and water vapour transfer, *Quart. J. Roy. Meteor. Soc.*, **106**, 85–100.

Wyngaard, J.C., O.R. Cote', and Y. Izumi, 1971: Local free convection, similarity and the budgets of shear stress and heat flux, *J. Atmos. Sci.*, **28**, 1171–1182.

Yang, K., N. Tamai, and T. Koike, 2001: Analytical solution of surface layer similarity equations, *J. Appl. Meteor.*, **40**, 1647–1653.

———, T. Koike, and D. Yang, 2003: Surface flux parameterization in the Tibetan Plateau, *Boundary-Layer Meteor.*, **106**, 245–262.